Geochemical Perspectives Letters

Continental crust had fully emerged by the end of the Paleoproterozoic

D. Mineart, S. Duncanson, W. Nachlas, B. Johnson

Supplementary Information

The Supplementary Information includes:

- Geologic Setting and Sample Descriptions
- Geochemical Methods
- Tracer Mass-balance Inverse Model
- Steady State Seawater Isotope Modelling
- Table S-1
- Figures S-1 to S-4
- Data Files S-1 to S-4
- Python Files S-1 to S-4

The Supplementary Information includes descriptions of the sample sites and lithologies, detailed description of the inverse tracer mass balance method, description of the steady state sea water model, and geochemical data including oxygen isotopes and chlorite geothermometry. The data can be downloaded as Excel files from the online version of this article at https://doi.org/10.7185/geochemlet.2551. We also provide all python code used for inversions, steady state modelling, and figure generation as python files.

Geologic Setting and Sample Descriptions

Sturgeon Lake Caldera Complex, NW Ontario, Canada

The Sturgeon Lake caldera is the first in three volcanic cycles, dated at about 2735 Ma (Franklin, 1977), located within the Sturgeon Lake greenstone belt. More broadly, the site is within the central part of the Wabigoon sub-province in the Archean Superior Province (Blackburn *et al.*, 1991). The volcanic cycles are primarily felsic, quartz-rich pyroclastic, and experienced multiple episodes of explosive eruptions and synvolcanic faulting (Davis and Trowell, 1982; Davis *et al.*, 1985). The volcanogenic massive sulfide (VMS) deposit occurrences increase towards the caldera and point towards an eastward migration of eruptive centers (Morton *et al.*, 1996). The caldera succession was subject to greenschist to lower amphibolite facies metamorphism (Franklin, 1977). Igneous and hydrothermal activity in the area lasted until around ~2738 Ma (Holk *et al.*, 2008)

A combined 451 samples and analyses of total outcrop and drill cores were collected in the original work from the Sturgeon Lake caldera complex, but only 402 samples and analyses were considered for this research (Holk *et al.*, 2008). The samples were fluorinated with BrF_5 and converted to CO_2 by reaction with a hot graphite rod. Determinations were analyzed on a Finnegan Mat 252 mass spectrometer using NBS-28 quartz as a standard, reported as 9.5±0.2‰. Analyses were completed at the Stable Isotope Laboratory of the Geological Survey of Canada (Ottawa). Samples from Darkwater, Pike Lake, and the Biedelman Bay intrusive complex (BBIC) were interpreted as the magma chamber for the Sturgeon Lake deposit (Galley *et al.*, 2000). The deposit experienced three primary modes of alteration: (a) high temperature (500-700 ºC) magmatic-hydrothermal alteration; (b) lower-temperature (300-400 ºC) seawater dominated, fracture controlled, subsolidus alteration; and (c) vein-and-fracture controlled alteration (Galley *et al.*, 2007; Holk *et al.*, 2008). Formation of the Darkwater gold deposit also post dates caldera-related hydrothermal activity, and was more actively associated with the last alteration type (Holk *et al.*, 2008). The magmatic-hydrothermal alteration event would generally produce distinct isotopic compositions of magmatic origin (about 5.7‰).

Starting rock $\delta^{18}O$ was estimated using analyses of zircons from across the area (King *et al.*, 2000). Zircons were isolated from nine different samples, ranging across both intrusive and extrusive members of the Sturgeon Lake complex. The average zircon $\delta^{18}O$ values from these samples is 5.4±0.3‰. The authors then calculate an estimated whole rock $\delta^{18}O$ value assuming equilibrium between magma and zircons at 800 ºC as a function of silica content. This produces whole rock estimated at between 6-8‰.

Temperatures for alteration at Sturgeon lake were estimated based on modelled mineral-pair oxygen isotope values (Holk et al., 2008). These authors presented a range of temperatures, based on different starting rock types and assumed fluid composition. We assigned an alteration temperature for each sample based on correlation between whole rock $\delta^{18}O$ and modelled temperatures.

Pecos Greenstone Belt, New Mexico, USA

We collected a total of fifty-five field samples were collected in Pecos (Fig. S-1), New Mexico, and 105 cores from the core library at the New Mexico Bureau of Geology and Mineral Resources. Field sample sites as listed: Tres Lagunas, Willow Creek, Pecos Canyon Road close to Dalton Picnic Site, and Spring Mountain Ridge off Elk Mountain Road (Fig. S-1). Core samples were drilled by the New Mexico Department of Technology and Mineral Resources (NMT). We collected cores from Willow Creek, Macho Canyon, and Jones Hill. We analysed samples from Willow Creek for this study. Sample lithologies, coordinates, and core details along with geochemical data are listed in the Data S-1 Excel file.

Sixteen samples were collected along Willow Creek and 30 cores from the New Mexico Bureau of Geology and Mineral Resources (NMT) core library. Samples collected ranged from metabasalt to andesite and diorite to metarhyolite. Some metabasalt samples contained phenocrysts of quartz or feldspar. Samples closer to the closed Willow Creek mine, which was actively mined as a VMS deposit, contained more visible grains of sulfides, and the float contained abundant micas and a few garnets.

Field and petrographic observations indicate a range of alteration, from intensely altered to somewhat altered. We collected from outcrops of that had altered volcanic characteristics, primarily mafic with some samples being intermediate to felsic, super fine-grained textures where grain size was indistinguishable by the naked eye. Some samples consisted of more felsic composition but were still very fine-grained. Willow Creek core samples from NMT were collected about every 100 ft from the top to the bottom of each core in order to

obtain a two-dimensional variability across the hydrothermal cell. Core samples ranged from coarse to very fine-grained, including mafic to intermediate to felsic compositions. Cores were drilled north of outcrop samples, inclined towards the Pecos mine (Fig. S-1).

Volcanic activity has been dated to 1720 Ma (Robertson and Condie, 1989). Subsequently, the Pecos area is thought to have experienced four major periods of deformation, with a compressional event that folded in a northeast trend, truncated by other structures and the Quaternary sediments. Poor exposures in the Pecos Mine area limit the ability to interpret if the folds experienced flexure-slip folding of a syncline, seen in other areas of Pecos, but it is probable that Willow Creek experienced the same regional process due to northeast-trending folds in the foliated granodiorites of the Pecos Mine areas (Riesmeyer, 1978).

The second major deformation event was the intrusion of the Late Precambrian Embudo granite, about 1.65 Ga. While this intrusion displaced and created discordant folding in other parts of Pecos, Willow Creek did not show evidence of significant structural disruption in the adjacent rocks.

The Pecos-Picuris Fault represents the final period of Precambrian deformation as a regional right-lateral strike-slip fault that cuts the Embudo granite in the Jones Mine area. A northeasterly-striking fault group in the Jones and Pecos Mine area may have been the master fault responsible for generating the Pecos-Picuris.

A final deformation period occurred as a late tensional event that faulted and displaced the Pennsylvanian and Precambrian rocks. The timing of the tensional event is not well constrained due to missing Cretaceous rocks in the area, but a proposed age by (Riesmeyer, 1978) was during the Oligocence-Miocene. The outcome of this event effectively dropped fault blocks on both sides of the Pecos River in a step-like fashion.

Geochemical Methods

Sample preparation

Samples were trimmed using a diamond saw blade to remove areas affected by weathering. A small cube (3x3x0.5 cm) was cut from each sample and then crushed into small shards using a jaw crusher, which was subsequently powdered in a shatterbox. The shatterbox container was made of tungsten carbide so as not to introduce any O-bearing material into sample powders. Eighteen billets were cut for polished thin sections, prepared by Spectrum Petrographics. The polished thin sections were used to determine the sample mineralogy using standard petrographic techniques and electron microprobe analyses.

Oxygen isotope analyses

We analysed Willow Creek whole-rock powder O isotopes using a standard laser fluorination technique using dual inlet on a Thermo Fisher MAT 253 Isotope Ratio Mass Spectrometer using reference gas calibrated to VSMOW (Sharp, 1990). We modified this procedure slightly by adding an ice bath surrounding the sample chamber to slow and prevent background fluorination of other samples not currently being heated by the CO_2 laser. Analyses were done at the University of New Mexico in the Centre for Stable Isotopes. Sample oxygen isotope measurements were compared to the San Carlos olivine (SCO) laboratory standard, calibrated to Vienna Standard Mean Ocean Water (VSMOW). The $\delta^{18}O$ obtained from repeated analysis of SCO was 5.32±0.6‰, relative to VSMOW. The accepted SCO $\delta^{18}O$ value is 5.26‰. For each sample, we counted sample gas between 10-30 cycles, resulting in sample uncertainty of ±0.1‰. Since this is less than the uncertainty from repeat analyses of SCO, we report sample uncertainties as ±0.6‰. Each sample was run once.

Chlorite geothermometry

We observed moderate amounts of bladed, Mg-rich chlorite in petrographic observation of thin sections, prevalent biotite-chlorite alteration, and abundant white mica replacing plagioclase (Fig. S-2). Such greenschist-facies assemblages are interpreted to reflect hydrothermal alteration temperatures of about 300 to 400 °C (Cathelineau, 1988; Jowett, 2021).

We performed geothermometry based on temperature dependence of the tetrahedral site occupancy in chlorite (Cathelineau, 1988; Jowett, 2021). The tetrahedral Al content and Mg/Mg+Fe ratio in chlorite is sensitive to crystallization temperature, and by measuring the composition of individual chlorite grains in texturally-significant locations of the samples, we provide quantitative estimates of the conditions of chlorite mineralization.

Measurements were performed using a Cameca SX-Five Field Emission Electron Probe Microanalyzer (FE-EPMA) at UW-Madison. Thirteen elements (Na, Mg, Si, Al, K, Ca, Ti, Cr, O, Fe, Mn, Ni, and Zn) were analysed on five spectrometers using LTAP, TAP, LPET, PC0, and LLIF diffraction crystals. Natural and synthetic standards were used for peaking and calibration: jadeite, natural; chlorite, var. clinochlore, natural; microcline, natural; wollastonite, natural; TiO_2, synthetic; Cr_2O_3, synthetic;; Fe_2O_3, natural; Mn_2SiO_4, synthetic; Ni_2SiO_4, synthetic; Zn_2SiO_4, natural. Measurements were made with accelerating voltage of 15 kV and beam current of 10 nA with 5 µm defocused beam. Seven slides were prepared for chlorite analysis, with three targeted grains, three to five points within each grain. Many measurements identified the presence of other phases such as amphibole, biotite, and white mica. Measurements of chlorite with analytical totals between 97-101.5 weight percent were accepted for thermometry calculations. Based on the observed correlation between measured $\delta^{18}O$ and calculated temperatures, we assigned an alteration temperature to each sample.

Previous modeling studies of fluid flow through hydrothermal systems indicate that most alteration occurs at peak fluid flow, which also typically correspond with peak temperatures (Wetzel *et al.*, 2001). We suggest, then, that O isotopes of altered rocks are mostly set at peak alteration conditions.

Tracer Mass-balance Inverse Model

As outlined in the main text, we applied an adapted tracer mass-balance inversion approach to estimate initial fluid $\delta^{18}O$ (Wunsch, 1996; Wing and Ferry, 2007; Johnson and Wing, 2020). The model code and data are available as supplementary files (Data S-1 to S-4 and Python S-1 to S-4), with the code available on the corresponding author's GitHub repository. The inverse model processes whole-rock oxygen isotope values and hydrothermal alteration temperatures from two-dimensional cross-sections of altered crust to estimate the fluid-to-rock ratio for a hydrothermal system.

To account for deformation in the Willow Creek samples and to reconstruct a two-dimensional cross-section, we oriented all samples relative to the hinge axis of a syncline fold. Horizontal distance was the distance from this hinge, while the vertical dimension was simply the elevation of the sample site.

During inversion, we assumed fluid and oxygen mass balance. The fluid mass balance assumption means there was no change in total fluid during hydrothermal alteration (i.e., no significant sink for water in hydrothermal minerals; (Johnson and Wing, 2020)) and implies that the amount of fluid entering the system is the same amount that leaves the system. Oxygen mass balance assumptions mean that the amount of oxygen in the rock will remain the same. Previous work calculated a negligible (no greater than 0.1‰) effect of the growth of hydrated minerals on initial fluid $\delta^{18}O$ estimates (Muehlenbachs and Clayton, 1976; Johnson and Wing, 2020;).

Steady State Seawater Isotope Modelling

We adapted a steady state seawater oxygen isotope model to describe potential pathways relating to continental emergence (Muehlenbachs, 1998). In this model, fluxes of the geologic water cycle, including low- and high-temperature hydrothermal circulation through the oceanic crust, terrestrial weathering, and recycling due to subduction, all have a characteristic isotopic fractionation between water and rock. Given flux (L/yr) inputs for each part of the geologic water cycle, we can calculate steady state seawater $\delta^{18}O$ (Table S-1).

The key forcing in our model is changing the continental weathering and growth water-rock fluxes (Fig. S-3). We either simulate a continuous increase in these fluxes from 0 to modern between 3-1 Ga, following proposed continental crust growth and cratonization (Reimink *et al.*, 2023; Reimink and Smye, 2024), or weight these fluxes relative to the abundance of detrital zircon age peaks.

For the zircon weighting approach, we calculated a detrended abundance for zircon ages in 30 Myr time bins (Puetz *et al.*, 2024), assuming a 97% survival rate for zircons from each bin (Puetz *et al.*, 2017). We then normalized detrended zircon abundance for each bin (Fig. S-4) to the most recent time bin, and multiplied continental weathering and growth by this normalisation.

Comparison with other seawater $\delta^{18}O$ reconstructions

First, it is possible either the sedimentary record or the altered ocean crust record do not record primary seawater conditions. Reactive transport modelling on hydrothermal circulation proposed that altered ocean crust oxygen isotopes are relatively insensitive to seawater $\delta^{18}O$, due to sluggish kinetic isotope exchange (Kanzaki, 2020). In detail, results of this modelling show a 2-D vertical profile of crust $\delta^{18}O$ is sensitive to different seawater $\delta^{18}O$, especially at shallow depths. Chemical sediments can be reset due to diagenetic effects, both associated with initial formation and burial and later events. Work has suggested that the progressive increase in $\delta^{18}O$ observed in a suite of chemical sediments could be due to stochastic alteration events. Yet, the coherency, at least in trend, between different chemical sedimentary records indicates the evolution of fluid or early depositional conditions over time.

Second, perhaps oceanic crust and chemical sediments record different parts of the marine environment. Oceanic crust is typically in contact with bottom water. It is possible that the chemical sedimentary record in the Proterozoic/Archean is biased towards continental margins. The processes of chemical sediment deposition might have changed substantially over time. While it is beyond the scope of this paper to reconcile the different trends observed, future work could try measuring multiple rock records (chemical sediment and altered ocean crust) from proximal locations of the same age as a first step.

There are have been a number of models that calculate seawater $\delta^{18}O$ over Earth history (Wallmann, 2001; Kasting *et al.*, 2006; Jaffrés *et al.*, 2007; Guo *et al.*, 2022). A commonality in these models is the assumption that the proportion of low- to high-temperature alteration in oceanic crust/lithosphere has changed over time, related to secular cooling of the mantle with decreased penetration of seawater to depth since the Archean (Kasting *et al.*, 2006; Jaffrés *et al.*, 2007; Guo *et al.*, 2022) or changes in weathering following the Neoproterozoic Snowball Earth glaciations (Wallmann, 2001). The net result of either process is an increase in seawater $\delta^{18}O$ over time, either much of Earth history or at least during the Phanerozoic.

While our work cannot speak directly to changes over the Phanerozoic, in sections of Precambrian altered ocean crust, the proportion of low- to high-temperature alteration appears to be similar to modern sections (Brauhart *et al.*, 1998; Holmden and Muehlenbachs, 1993). We therefore suggest that this balance/buffering has been consistent over time (Gregory, 1991; Muehlenbachs, 1998).

Supplementary Tables

Table S-1 Steady state water-rock fluxes and isotopic exchange, after Muehlenbachs (1998).

Flux	[(O-process/yr)/O-ocean]*10^9	Fractionation between rock and water (‰)
Continental weathering	Varies, modern = 8	12
Continental growth	Varies, modern = 1.2	1.2
Water recycling during subduction	0.6	2.5
Low-temperature hydrothermal alteration/seafloor weathering	1.7	9.3
High-temperature hydrothermal alteration	14.6	1.5 to 4.1 between 3 to 1 Ga

Supplementary Figures

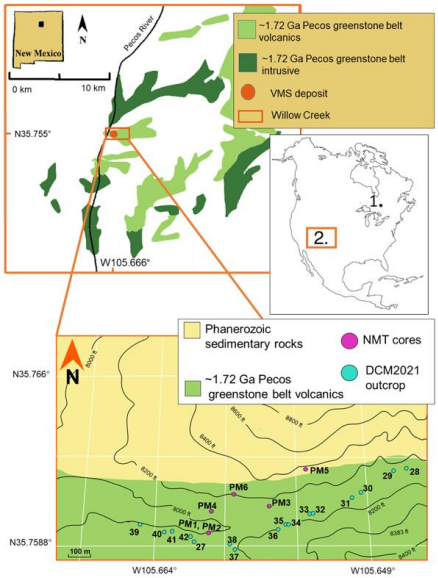

Figure S-1 North America map (centre-right) showing sample locations: (1) Sturgeon Lake and (2) the Pecos Greenstone Belt. The adapted geologic map of Pecos, NM from (Slack *et al.*, 2009) (upper-left), shows the distribution of greenstone belts and the location of the Willow Creek deposit, with a zoomed-in map of the Willow Creek deposit (bottom-centre). Core drill sites PM1 through PM6 (magenta dots) are plotted north of outcrop samples (turquoise dots). The Pecos Mine is situated just west of samples. All samples are from the 1.72 Ga Pecos greenstone belt volcanics, with PM5 containing Phanerozoic cover rocks.

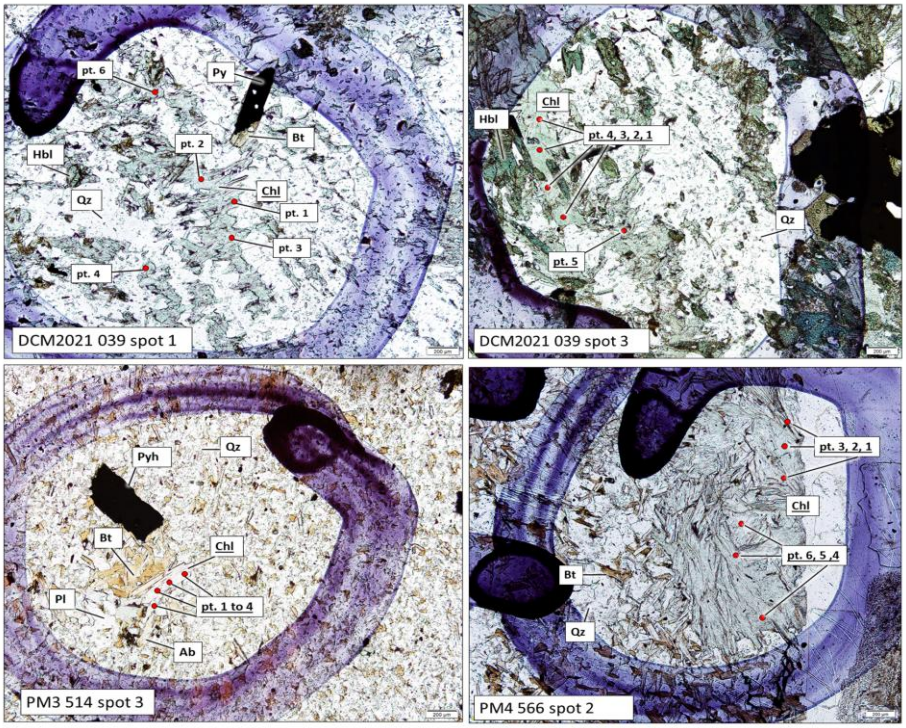

Figure S-2 Example thin section images showing chlorite used for geothermometry. Thin section images were taken at 2x magnification of samples DCM2021 039 spot 1 and 3 (top), PM3 514 spot 3 (bottom left), and PM4 566 spot 2 (bottom right). Red circles represent spot analysis (~10 microns). Mineral abbreviations: Chl (chlorite), Bt (biotite), Qz (quartz), Pl (plagioclase), Hbl (hornblende), Py (pyrite), Pyh (pyrrhotite). Small scale bar in lower right of each image is 200 microns.

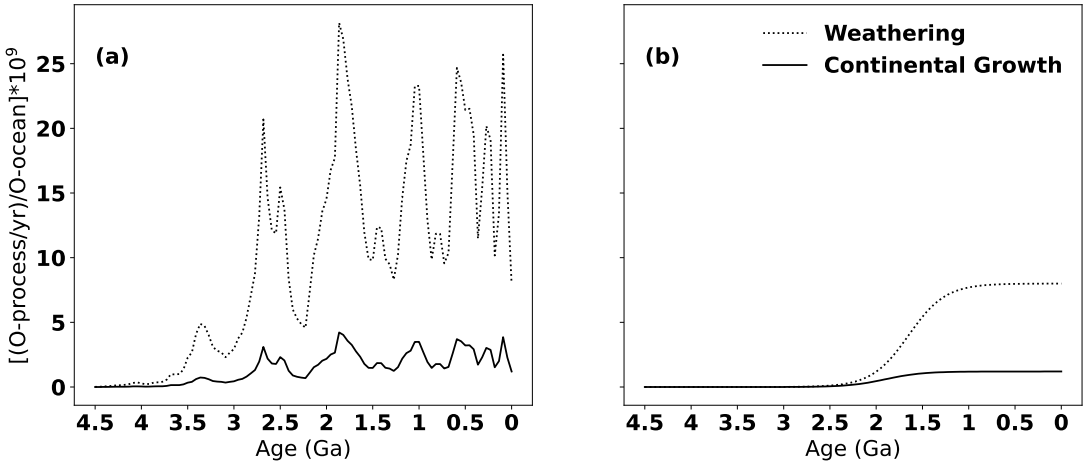

Figure S-3 Continental weathering and growth water-rock fluxes for either **(a)** Zircon-weighted or **(b)** continuous growth steady state models described in the text. Units are in moles O per 10^9 years normalized to the modern amount of O in the oceans.

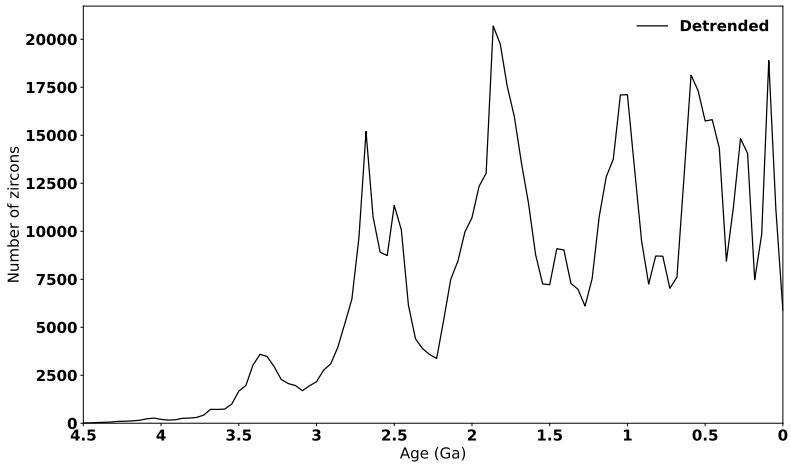

Figure S-4 Zircon age histogram and detrended values in 30 Myr bins. Data from (Puetz *et al.*, 2024).

Supplementary Data and Python Code Files

All data files (xlsx) and Python code files can be downloaded from the online version of this article at https://doi.org/10.7185/geochemlet.2551.

Data S-1 Oxygen isotope analyses of samples from the Pecos greenstone belt, including estimated temperatures of alteration based on the chlorite data in Data S-2.

Data S-2 Major element analyses of chlorite samples from electron microprobe at the University of Wisconsin Madison.

Data S-3 Oxygen isotope analyses from the Sturgeon Lake caldera used in the inversion. Data are from Holk *et al.* (2008).

Data S-4 Compiled detrital zircon age dataset from Puetz *et al*. (2024) used in Figure 4.

Python S-1 inversion_wrapper.py – Python script that reads in data, calls the inversion file (o_isotope_inversion.py), calculates seawater $\delta^{18}O$ over time, and produces the figures seen in the main manuscript.

Python S-2 o_isotope_invert.py – python script that contours and inverts data from hydrothermal sections to calculate starting fluid $\delta^{18}O$.

Python S-3 nan_helper.py – python script to help remove nans from matrices.

Python S-4 matrix_average.py – function to take matrix input and calculate average value between all entries.

Supplementary Information References

Blackburn, C.E., Johns, G.W., Ayer, J., Davis, D.W. (1991) Wabigoon subprovince. *Geology of Ontario* 4, 303–381.

Brauhart, C.W., Groves, D.I., Morant, P. (1998) Regional alteration systems associated with volcanogenic massive sulfide mineralization at Panorama, Pilbara, Western Australia. *Economic Geology* 93, 292–302. https://doi.org/10.2113/gsecongeo.93.3.292

Cathelineau, M. (1988) Cation site occupancy in chlorites and illites as a function of temperature. *Clay Minerals* 23, 471–485. https://doi.org/10.1180/claymin.1988.023.4.13

Davis, D.W., Krogh, T.E., Hinzer, J., Nakamura, E. (1985) Zircon dating of polycyclic volcanism at Sturgeon Lake and implications for base metal mineralization. *Economic Geology* 80, 1942–1952. https://doi.org/10.2113/gsecongeo.80.7.1942

Davis, D.W., Trowell, N.F. (1982) U–Pb zircon ages from the eastern Savant Lake – Crow Lake metavolcanic–metasedimentary belt, northwest Ontario. *Canadian Journal of Earth Sciences* 19, 868–877. https://doi.org/10.1139/e82-072

Franklin, J. (1977) Stratigraphic and chemical relations, south Sturgeon Lake area. Geotraverse Conference 1977, 118–120.

Galley, A., Breemen, O.V., Franklin, J. (2000) THE RELATIONSHIP BETWEEN INTRUSION-HOSTED Cu-Mo MINERALIZATIONAND THE VMS DEPOSITS OF THE ARCHEAN STURGEON LAKE MINING CAMP, NORTHWESTERNONTARIO. *Economic Geology* 95, 1543–1550.

Galley, A.G., Hannington, M.D., Jonasson, I.R. (2007) Volcanogenic massive sulphide deposits. *Mineral Deposits of Canada: A Synthesis of Major Deposit-Types, District Metallogeny, the Evolution of Geological Provinces, and Exploration Methods*. Geological Association of Canada, Mineral Deposits Division, 141–161.

Gregory, R. (1991) Oxygen isotope history of sea- water revisited: 3.5 billion years of the greenstone record and its implication for the stability of seawater 180. *Stable Isotope Geochemistry: a Tribute to Samuel Epstein. Geochemical Society, Special Publication* 3, 65–76.

Guo, M., Wostbrock, J.A.G., Planavsky, N.J., Korenaga, J. (2022) Reconstructing seawater δ18O and Δ′17O values with solid Earth system evolution. *Earth and Planetary Science Letters* 592, 117637. https://doi.org/10.1016/j.epsl.2022.117637

Holk, G.J., Taylor, B.E., Galley, A.G. (2008) Oxygen isotope mapping of the Archean Sturgeon Lake caldera complex and VMS-related hydrothermal system, Northwestern Ontario, Canada. *Mineralium Deposita* 43, 623–640. https://doi.org/10.1007/s00126-008-0185-3

Holmden, C., Muehlenbachs, K. (1993) The $^{18}O/^{16}O$ Ratio of 2-Billion-Year-Old Seawater Inferred from Ancient Oceanic Crust. *Science* 259, 1733–1736. https://doi.org/10.1126/science.259.5102.1733

Jaffrés, J.B.D., Shields, G.A., Wallmann, K. (2007) The oxygen isotope evolution of seawater: A critical review of a long-standing controversy and an improved geological water cycle model for the past 3.4 billion years. *Earth-Science Reviews* 83, 83–122. https://doi.org/10.1016/j.earscirev.2007.04.002

Johnson, B.W., Wing, B.A. (2020) Limited Archaean continental emergence reflected in an early Archaean 18O-enriched ocean. *Nature Geoscience* 13, 243–248. https://doi.org/10.1038/s41561-020-0538-9

Jowett, E.C. (2021) Fitting Iron and Magnesium into the Hydrothermal Chlorite Geothermometer. *SSRN Electronic Journal*.

Kanzaki, Y. (2020) Quantifying the buffering of oceanic oxygen isotopes at ancient midocean ridges. *Solid Earth* 11, 1475–1488. https://doi.org/10.1016/j.epsl.2006.09.029

Kasting, J.F., Howard, M.T., Wallmann, K., Veizer, J., Shields, G., Jaffrés, J. (2006) Paleoclimates, ocean depth, and the oxygen isotopic composition of seawater. *Earth and Planetary Science Letters* 252, 82–93. https://doi.org/10.1016/j.epsl.2006.09.029

King, E.M., Valley, J.W., Davis, D.W. (2000) Oxygen isotope evolution of volcanic rocks at the Sturgeon Lake volcanic complex, Ontario. *Canadian Journal of Earth Sciences* 37, 39–50. https://doi.org/10.1139/e99-106

Morton, R., Hudak, G., Koopman, E. (1996) Physical volcanology, hydrothermal alteration and massive-sulphide deposits of the Sturgeon Lake caldera. *Geological Association of Canada, Winnipeg Section, Field trip guidebook B* 3, 27–29.

Muehlenbachs, K. (1998) The oxygen isotopic composition of the oceans, sediments and the seafloor. *Chemical Geology* 145, 263–273. https://doi.org/10.1016/S0009-2541(97)00147-2

Muehlenbachs, K., Clayton, R.N. (1976) Oxygen isotope composition of the oceanic crust and its bearing on seawater. *Journal of Geophysical Research* 81, 4365–4369. https://doi.org/10.1029/JB081i023p04365

Puetz, S.J., Condie, K.C., Pisarevsky, S., Davaille, A., Schwarz, C.J., Ganade, C.E. (2017) Quantifying the evolution of the continental and oceanic crust. *Earth-Science Reviews* 164, 63–83. https://doi.org/10.1016/j.earscirev.2016.10.011

Puetz, S.J., Spencer, C.J., Condie, K.C., Roberts, N.M.W. (2024) Enhanced U-Pb detrital zircon, Lu-Hf zircon, δ18O zircon, and Sm-Nd whole rock global databases. *Scientific Data* 11, 56. https://doi.org/10.1038/s41597-023-02902-9

Reimink, J.R., Smye, A.J. (2024) Subaerial weathering drove stabilization of continents. *Nature* 629, 609–615. https://doi.org/10.1038/s41586-024-07307-1

Reimink, J.R., Davies, J.H.F.L., Moyen, J.-F., Pearson, D.G. (2023) A whole-lithosphere view of continental growth. *Geochemical Perspectives Letters* 26, 45–49. https://doi.org/10.7185/geochemlet.2324

Riesmeyer, W.D. (1978) Precambrian geology and ore deposits of the Pecos mining district, San Miguel and Santa Fe Counties, New Mexic. PhD Thesis, University of New Mexico. https://doi.org/10.56577/FFC-30.175

Robertson, J.M., Condie, K.C. (1989) Geology and geochemistry of early Proterozoic volcanic and subvolcanic rocks of the Pecos greenstone belt, Sangre de Cristo Mountains, New Mexico. *Geological Society of America Special Papers*. Geological Society of America, 119–146. https://doi.org/10.1130/SPE235-p119

Sharp, Z.D. (1990) A laser-based microanalytical method for the in situ determination of oxygen isotope ratios of silicates and oxides. *Geochimica et Cosmochimica Acta* 54, 1353–1357. https://doi.org/10.1016/0016-7037(90)90160-M

Slack, J.F., Grenne, T., Bekker, A. (2009) Seafloor-hydrothermal Si-Fe-Mn exhalites in the Pecos greenstone belt, New Mexico, and the redox state of ca. 1720 Ma deep seawater. *Geosphere* 5, 302–314. https://doi.org/10.1130/GES00220.1

Wallmann, K. (2001) The geological water cycle and the evolution of marine δ 18 O values. *Geochimica et Cosmochimica Acta* 65, 2469–2485. https://doi.org/10.1016/S0016-7037(01)00603-2

Wetzel, L.R., Raffensperger, J.P., Shock, E.L. (2001) Predictions of hydrothermal alteration within near-ridge oceanic crust from coordinated geochemical and fluid flow models. *Journal of Volcanology and Geothermal Research* 110, 319–341. https://doi.org/10.1016/S0377-0273(01)00215-3

Wing, B.A., Ferry, J.M. (2007) Magnitude and geometry of reactive fluid flow from direct inversion of spatial patterns of geochemical alteration. *American Journal of Science* 307, 793–832. https://doi.org/10.2475/05.2007.02

Wunsch, C. (1996) *The ocean circulation inverse problem*. Cambridge University Press, Cambridge. https://doi.org/10.1017/CBO9780511629570